frontiers in Earth Science

ORIGINAL RESEARCH
published: 16 February 2022
doi: 10.3389/feart.2022.821367

Evaluation of the Rock Uplift Pattern in the Central Yunnan Subblock, SE Tibetan Plateau: Based on the Bedrock Channel Profile

*Liang Yu, Youpu Dong *, Weiwei Zhou *, Dongyue Zhang, Dan Wang, Huayu Yu, Yangyang Ren and Jiangtao Li*

Faculty of Land Resource Engineering, Kunming University of Science and Technology, Kunming, China

The uplift pattern of the southeastern Tibetan Plateau is strongly related to the topographic evolution stemming from the India–Eurasia collision. However, whether strain is localized along major faults that bound large tectonic blocks or is accommodated across regions has been strongly debated. In this study, we used stream power incision models to obtain the distribution pattern of the channel steepness indices to understand the rock uplift pattern across the area, as increased channel steepness indices often correlate with the rock uplift rates. In this study, the river longitudinal profiles were analyzed to obtain the distribution of the channel steepness indices in the Central Yunnan subblock. The results suggested very weak correlations between the steepness indices and the lithology, precipitation, sediment flux, or channel concavity indices. Along the Xiaojiang strike–slip fault and the interior subblock, the uplift rate was slower, while the northern part had uplifted faster and was controlled by thrust fault systems. The channel steepness increased gradually from south to north. Thus, the distribution pattern of the normalized channel steepness, k_{sn}, index within the Central Yunnan subblock provides notable support for the argument for the thrusting transformation-limited extrusion model of the Tibetan Plateau.

Keywords: stream power incision model, channel steepness index, the Central Yunnan subblock, river longitudinal profile, rock uplift

OPEN ACCESS

Edited by:
Rong Yang,
Zhejiang University, China

Reviewed by:
Lei Wu,
Zhejiang University, China
Yang Wang,
Sun Yat-sen University, China

****Correspondence:***
Youpu Dong
dongypsd@126.com
Weiwei Zhou
605316200@qq.com

Specialty section:
This article was submitted to Quaternary Science, Geomorphology and Paleoenvironment, a section of the journal Frontiers in Earth Science

Received: *24 November 2021*
Accepted: *07 January 2022*
Published: *16 February 2022*

Citation:
Yu L, Dong Y, Zhou W, Zhang D, Wang D, Yu H, Ren Y and Li J (2022) Evaluation of the Rock Uplift Pattern in the Central Yunnan Subblock, SE Tibetan Plateau: Based on the Bedrock Channel Profile. Front. Earth Sci. 10:821367. doi: 10.3389/feart.2022.821367

INTRODUCTION

The Tibetan Plateau is one of the most studied natural laboratories for examination of the relationship between continental collision and landscape evolution (Clark et al., 2005; Clark, 2012; Allen et al., 2013; Zheng et al., 2013; Liu et al., 2008; Molnar and England, 1990; Liu-Zeng et al., 2018; Wang et al., 2019). Although there has been much work done in the region, it is still poorly understood how the southeastern margin of the Tibetan Plateau responded to the India–Eurasia continental collision. Additionally, whether the strain is mainly localized along the boundary faults of large blocks (Tapponnier, 2001) or accommodated within the block (Houseman and England, 1993; Royden et al., 1997; Clark et al., 2005; Clark et al., 2004; Wang et al., 2017) has been strongly debated.

Research on the bedrock channel fluvial systems has examined the relationships between climate variations, surface processes, and tectonic evolution (Raymo and Ruddiman, 1992; Hartshorn et al., 2002; Dibiase and Whipple, 2011; Ferrier et al., 2013; Dibiase, 2014; Finnegan et al., 2014; Pan et al.,

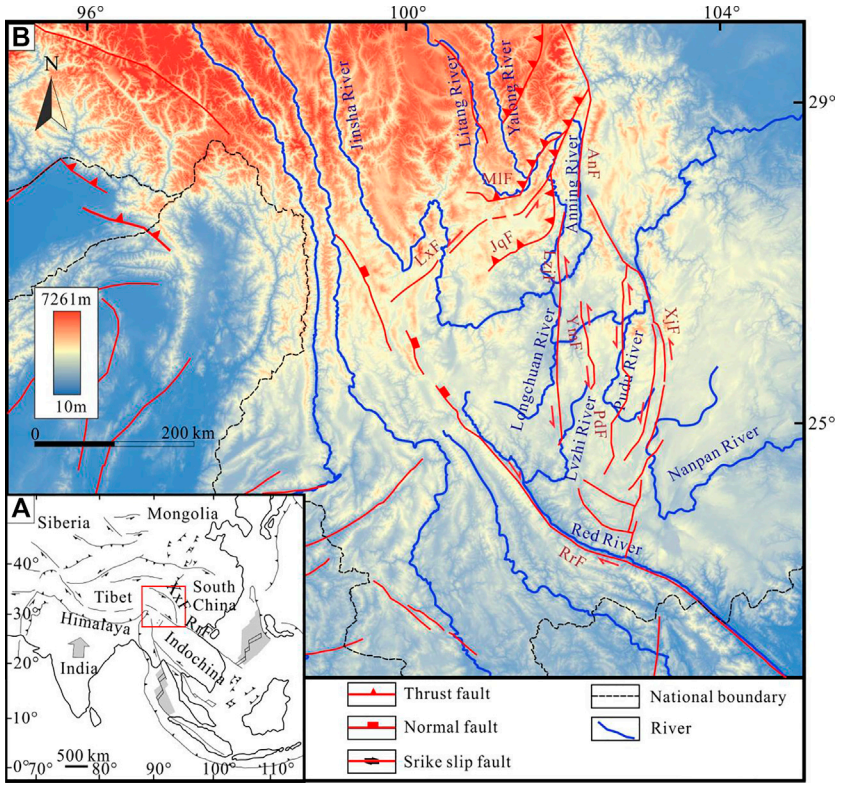

FIGURE 1 | Topographic map of the Central Yunnan subblock. **(A)** Location of the study area. **(B)** Topography, major faults, and rivers in the southeastern Tibetan Plateau. *XxF*, Xianshuihe–Xiaojiang Fault; *AnF*, Anninghe Fault; *LxF*, Lijiang–Xiaojinhe Fault; *MlF*, Muli Fault; *JqF*, Jinhe–Qinghe Fault; *LzjF*, Lvzhijiang Fault; *YmF*, Yimen Fault; *PdF*, Pudu Fault; *XjF*, Xiaojiang Fault; *RrF*, Red River Fault.

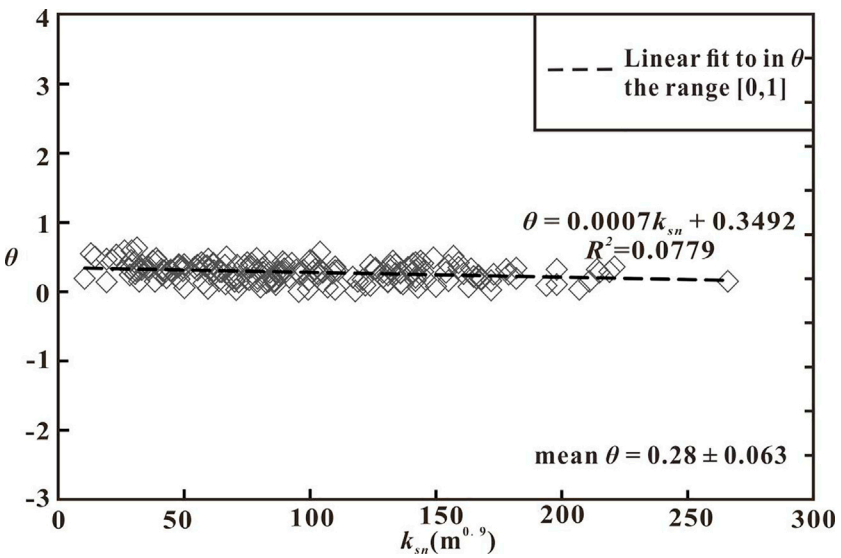

FIGURE 2 | Normalized channel steepness calculated for a reference concavity (θ_{ref} = 0.45) plotted against the actual concavity (θ) of the profile. The streams extracted for river profile analysis and the steepness and concavity indices of each segment are in the *Supplementary File*.

2015; Kirby and Ouimet, 2011; Kirby et al., 2007; Lave and Avouac, 2001) and has been used to interpret the relationships between topography, elevation, and denudation rates (Pritchard et al., 2009; Schwanghart and Scherler, 2020). In this study, we selected the Central Yunnan subblock as our study area (**Figure 1**). We extracted longitudinal river profiles from 320

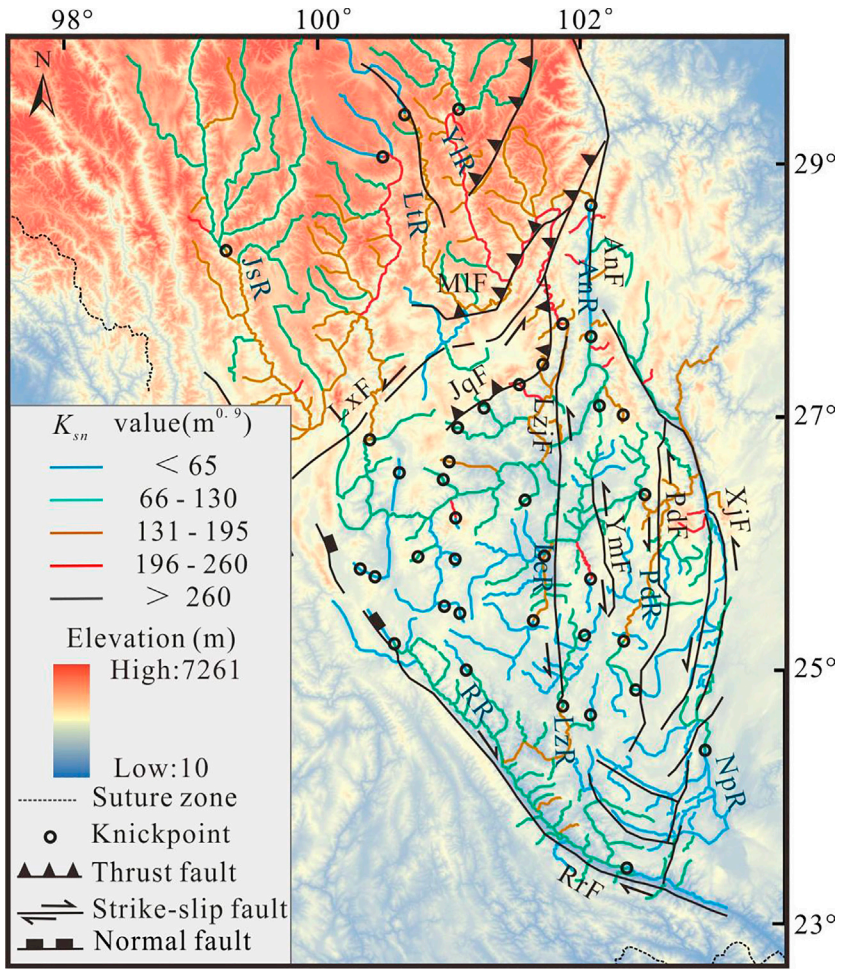

FIGURE 3 | Spatial pattern of the normalized channel steepness across the Central Yunnan subblock. *AnF*, Anninghe Fault; *LxF*, Lijiang–Xiaojinhe Fault; *MlF*, Muli Fault; *JqF*, Jinhe–Qinghe Fault; *LzjF*, Lvzhijiang Fault; *YmF*, Yimen Fault; *PdF*, Pudu Fault; *XjF*, Xiaojiang Fault; *RrF*, Red River Fault; *AnR*, Anning River; *LcR*, Longchuan River; *PuR*, Pudu River; *LzR*, Lvzhi River; *NpR*, Nanpan River; *RrR*, Red River; *JsR*, Jinsha River; *LtR*, Litang River.

rivers and calculated the channel steepness indices and concavities to determine the uplift patterns in this area (e.g., Kirby and Whipple, 2001; Whipple, 2004; Wobus et al., 2006; Oskin et al., 2014; Su et al., 2016) based on the digital elevation model data of the 90-m Shuttle Radar Topography Mission (downloaded from http://srtm.csi.cgiar.org/) by ArcGIS 10.2 and MATLAB R2015b. Thereafter, the influence of lithology resistance, precipitation, and sediment flux on channel steepness indices was analyzed to obtain the distribution pattern of the rock uplift within the subblock.

Regional Setting

The Sichuan–Yunnan rhombic block is located in the southeastern margin of the Tibetan Plateau. The Lijiang–Xiaojinhe Fault cuts the block into two parts: the Central Yunnan subblock in the south and the northwestern Sichuan subblock in the north (Xu et al., 2003) (**Figure 1**). In this paper, we mainly studied the Central Yunnan subblock.

The average elevation of the Central Yunnan subblock is about 2,000 m. The geotectonic location belongs to the southeastern margin of the Tibetan Plateau. It is adjacent to the Simao block in the south and the Caledonian fold belt in southeastern Yunnan to the east (Huangfu and Qin, 2006; He et al., 2009; Wang et al., 2015). For most parts of the area, annual rainfall ranges from 600 to 1,100 mm and gradually increases from north to south. Owing to the abundant rainfall, the study area has developed a dense river network, with many large rivers originating in the area (e.g., Longchuan River, Red River, Nanpan River, Pudu River, Anning River, and Xiaohedi River) (**Figure 1**).

The lithology of the central region of the subblock is relatively homogenous (consisting of Cretaceous–Jurassic sandstones and mudstones), while the lithology of the border region of the Central Yunnan subblock is complex (including Paleozoic shales, schists, and gneiss, Cambrian limestones and dolomites, and Triassic phyllites and mudstones). The subblock is

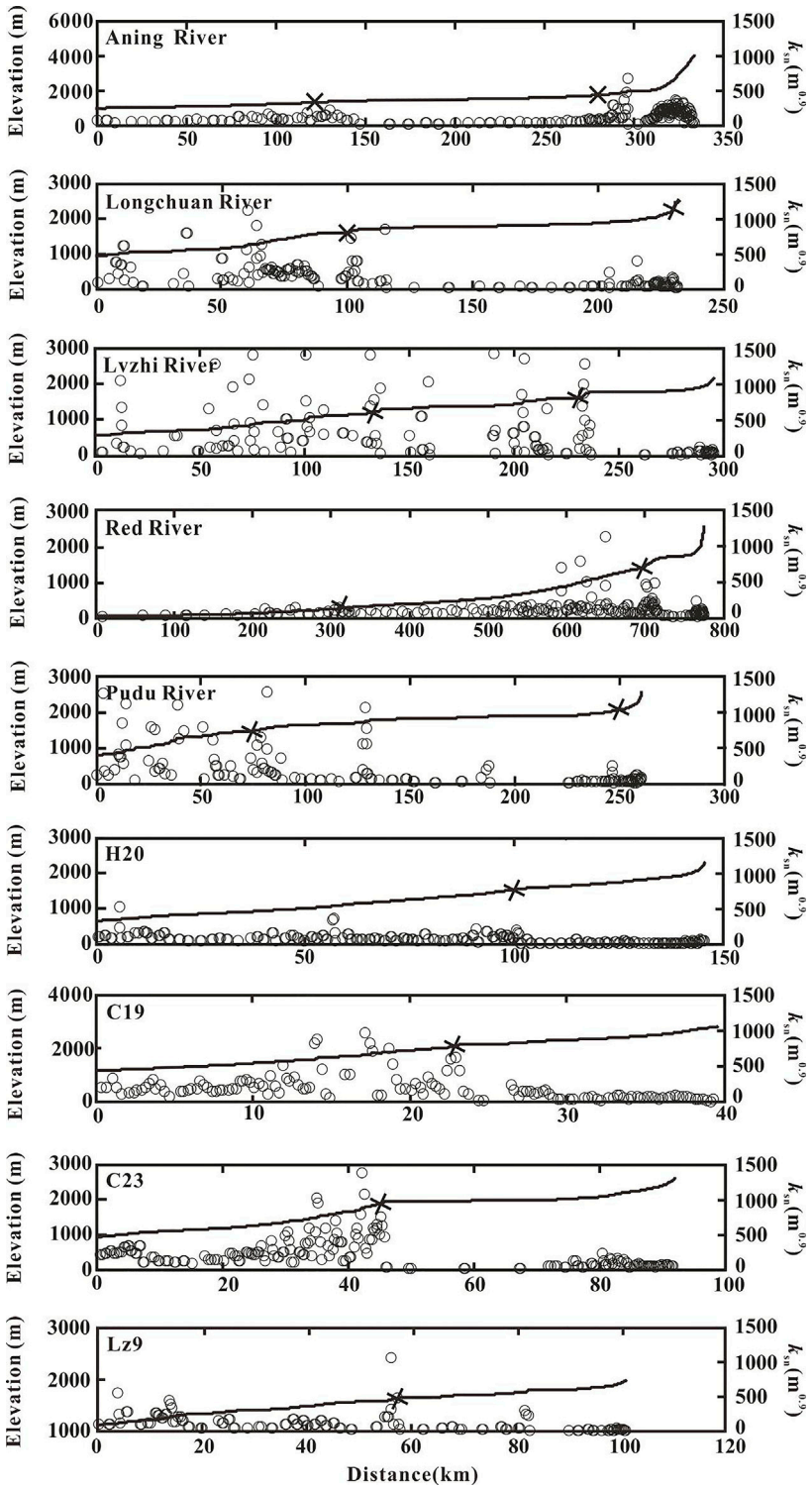

FIGURE 4 | Channel steepness of representative river profiles. *Black crosses* are knickpoints.

constrained by the Xiaojiang Fault, Lijiang–Xiaojinhe Fault, and the Red River Fault. The northern region of the block is cut by a series of thrust faults (the Jiulong, the Muli, and Jinhe–Qinghe thrusting faults) (**Figure 1**). The central region of the block is cut by a series of strike–slip faults (the Xiaojiang, Lvzhijiang, and Yimen strike–slip faults) (**Figure 1**).

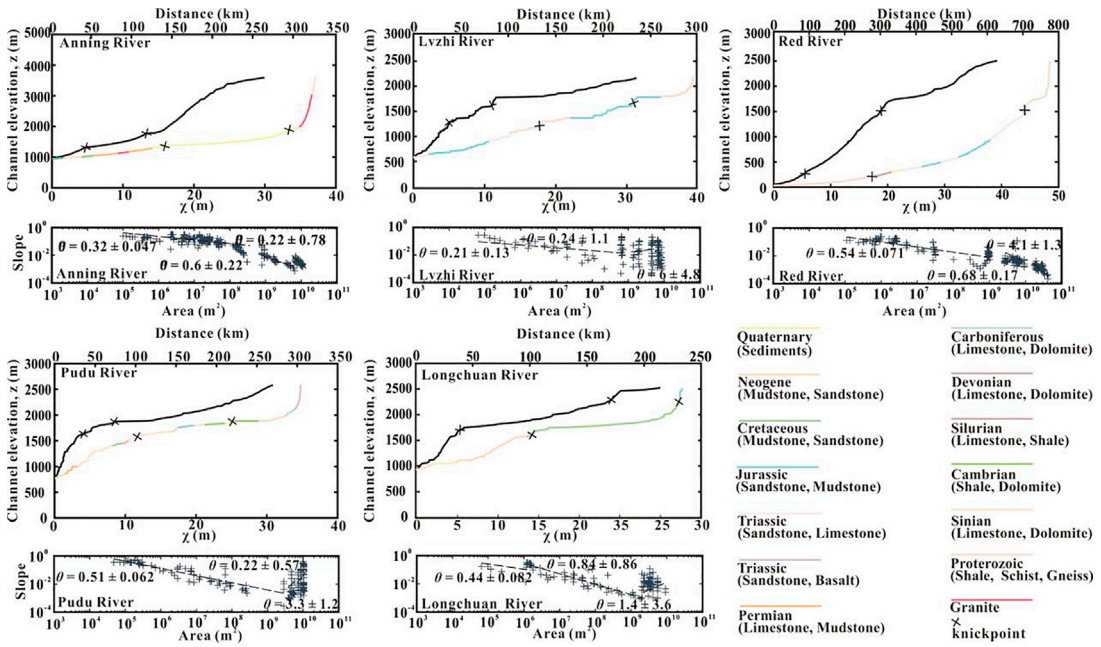

FIGURE 5 | Stream profile analysis for the trunk rivers of the five large drainage basins. The *colored curve* is a river profile with variable lithologies.

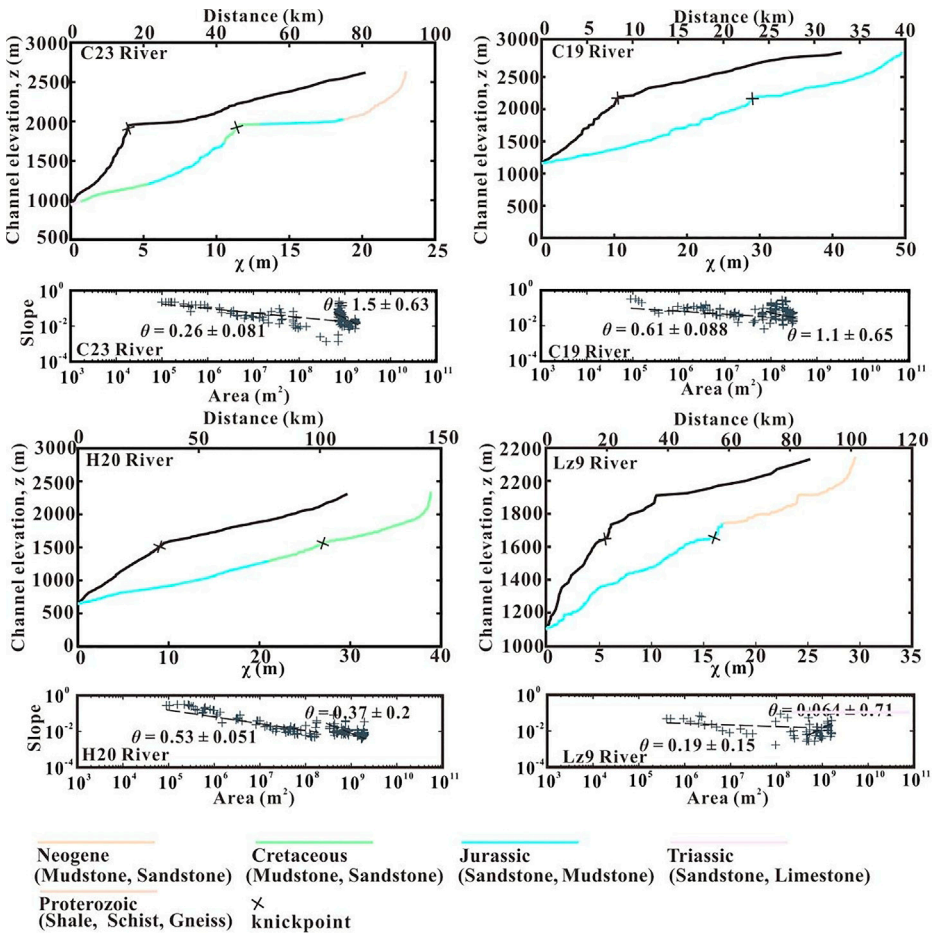

FIGURE 6 | Stream profile analysis for the four middle-scale rivers. The *colored curve* is a river profile with variable lithologies.

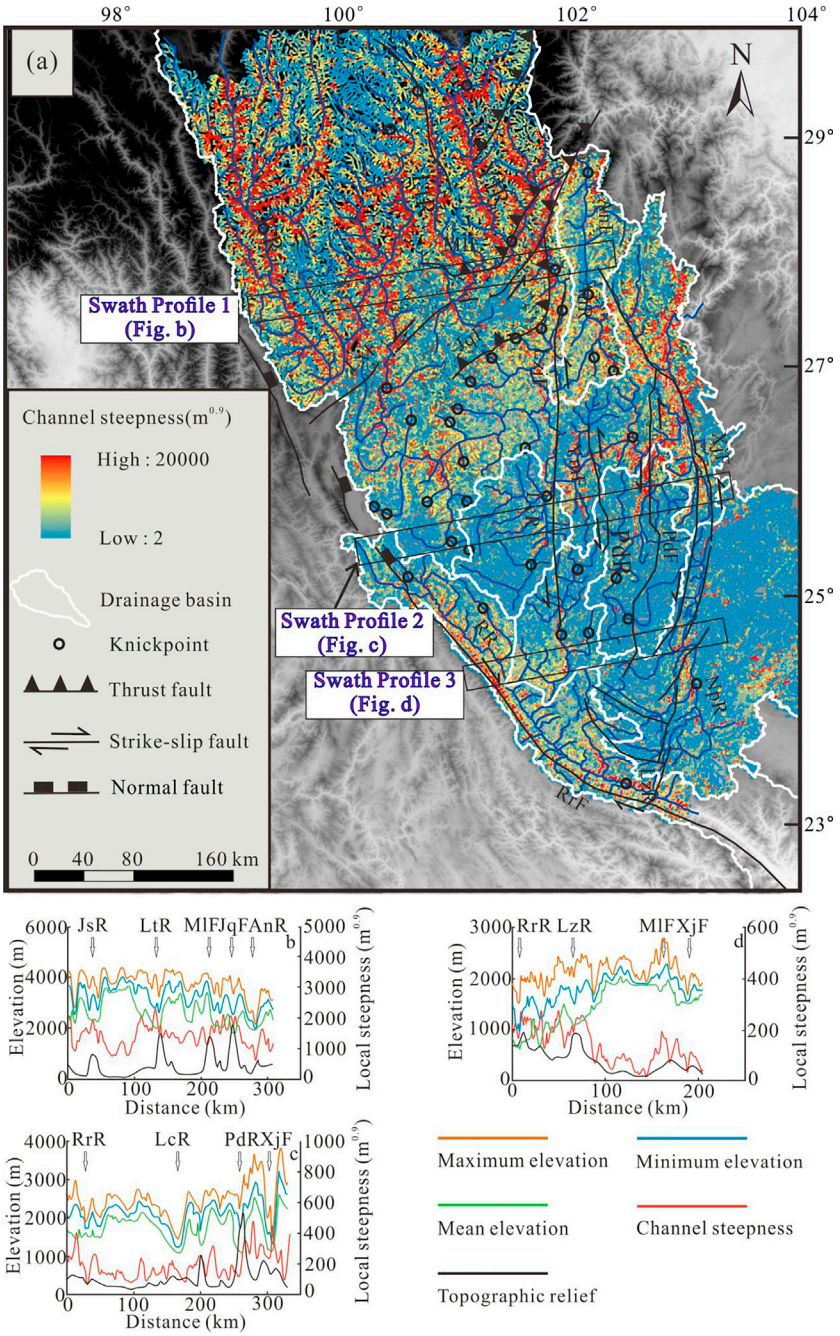

FIGURE 7 | (**A**) Map of local channel steepness values calculated under an elevation interval of 100 m. **(B–D)** Geological cross-sections and swath profiles of the elevation and local channel steepness indices along the section in **(A)**: swath profile 1 **(B)**; swath profile 2 **(C)**; and swath profile 3 **(D)**. The maximum, minimum, mean elevation, and topographic relief are shown in *orange*, *green*, *blue*, and *red*, respectively. Major faults and rivers are as follows: *RrR*, Red River; *LtF*, Litang Fault; *MlF*, Muli Fault; *JqF*, Jinhe–Qinghe Fault; *JsR*, Jinsha River; *LtR*, Litang River; *LcR*, Longchuan River; *LzR*, Lvzhi River; *PdR*: Pudu River; *XjR*, Xiaojiang River. Average local steepness indices are shown in *black*.

In the Cenozoic, most of the fault zones and orogenic belts of the Tibetan Plateau were active due to the strong collision between India and Eurasia (Wang et al., 2012; Shen et al., 2016; Zhang et al., 2016; Zhang et al., 2017; Liu-Zeng et al., 2018). The Xianshuihe–Xiaojiang Fault is a very large left lateral strike–slip fault (e.g., Xiang et al., 2002; Li and Zhang, 2013; Yan and Lin, 2015; Xu et al., 2007). In the Late Cenozoic, the Xianshuihe–Xiaojiang Fault offset the NE–SW Longmenshan thrust fault by as much as 60 km, splitting it into the north Longmenshan (NLM) and south Longmenshan (SLM) thrust

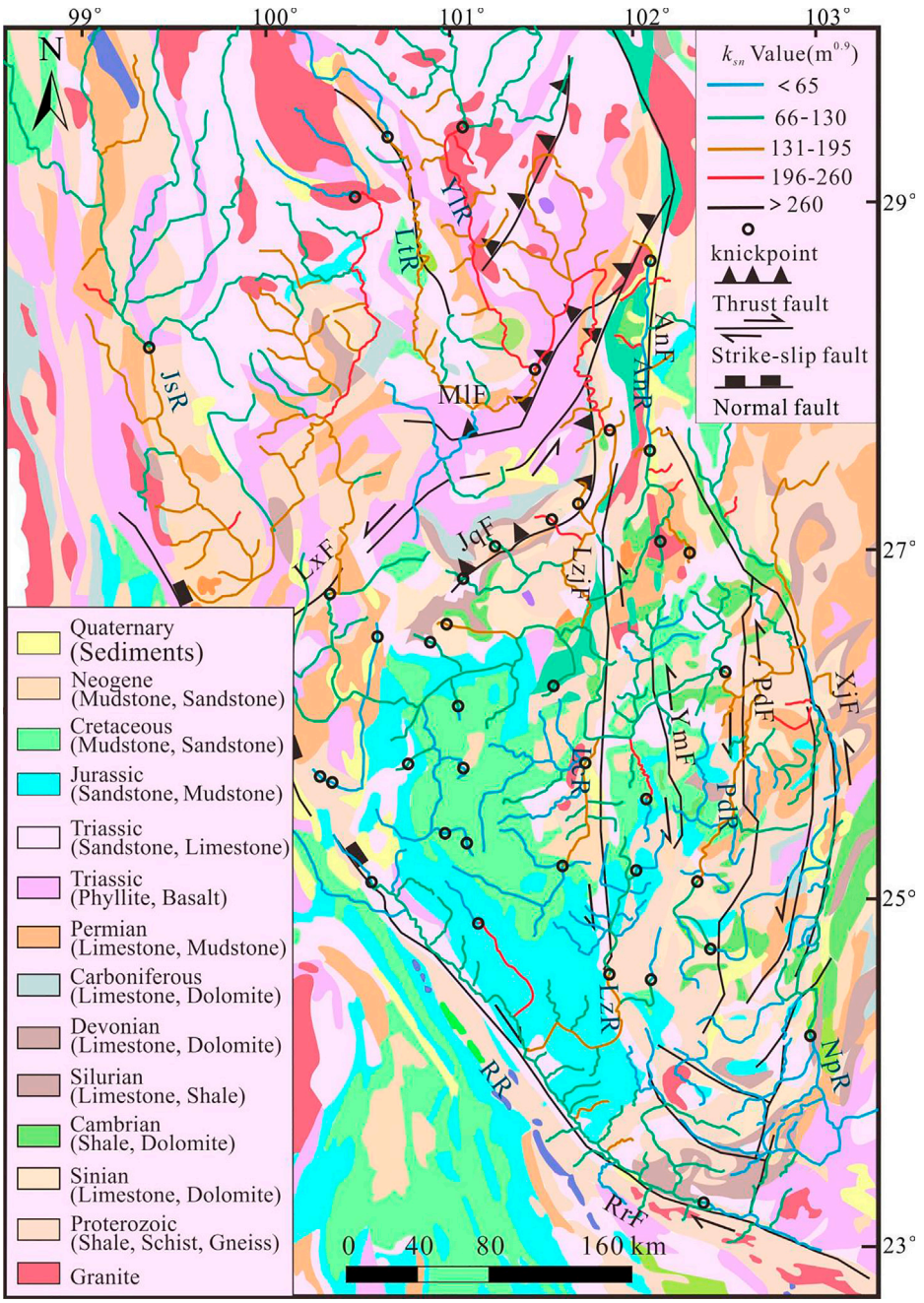

FIGURE 8 | Comparison of normalized channel steepness (k_{sn}) to lithologic variability in the Central Yunnan subblock. *AnF*, Anninghe Fault; *LxF*, Lijiang–Xiaojinhe Fault; *MlF*, Muli Fault; *JqF*, Jinhe–Qinghe Fault; *LzjF*, Lvzhijiang Fault; *YmF*, Yimen Fault; *PdF*, Pudu Fault; *XjF*, Xiaojiang Fault; *RrF*, Red River Fault; *AnR*, Anning River; *LcR*, Longchuan River; *PuR*, Pudu River; *LzR*, Lvzhi River; *NpR*, Nanpan River; *RrR*, Red River; *JsR*, Jinsha River; *LtR*, Litang River.

belts (Burchfiel et al., 1995; Wang et al., 1998). The SLM includes the Muli Fault, Lijiang–Xiaojinhe Fault, and Jinhe–Qihe Fault (Yin et al., 2020; Wang et al., 2012).

The uplift history and the expansion of the southeastern margin of the Tibetan Plateau have been studied intensely using several methods. Analysis of the ^{18}O isotopes of carbonate rocks in Cenozoic sedimentary basins (Li et al., 2015; Tang et al., 2017; Hoke, 2018) interpreted that the palaeo-elevation of the southeastern margin of the plateau reached its present height prior to the Eocene. In addition, episodic periods of uplifts have occurred in the region since the Late Cenozoic, determined through various thermochronometers (e.g., Xu and Kamp, 2000; Chen et al., 2006; Wilson and Fowler, 2011; Wang et al., 2012; Tian et al., 2013, Tian et al., 2014, Tian et al., 2015; Shen et al., 2016; Zhang et al., 2016; Zhang et al., 2017; Liu-Zeng et al., 2018; Wu et al., 2020).

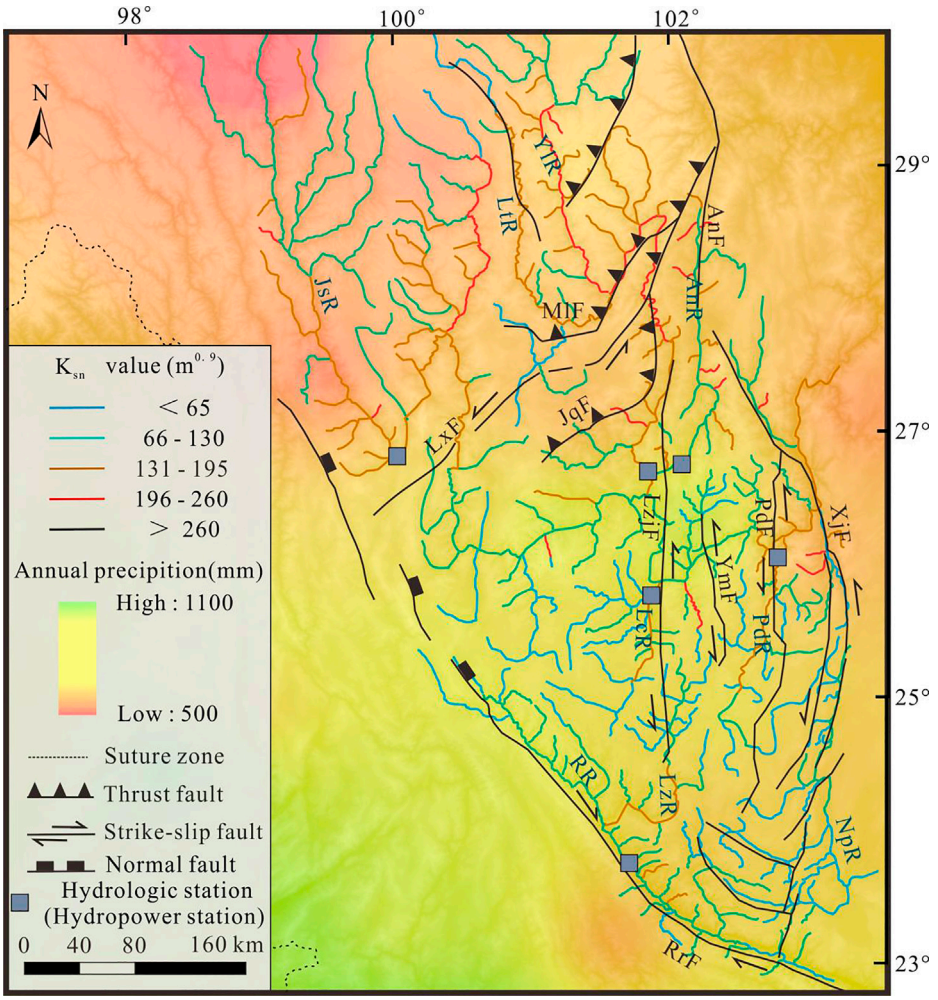

FIGURE 9 | Comparison of normalized channel steepness (k_{sn}) to annual precipitation in the Central Yunnan subblock. The precipitation data (timescale: from 1970 to 2019) were downloaded from http://data.cma.cn. The tributary catchments (*white boundary*) were selected randomly for correlation analysis between channel steepness with precipitation and drainage area. *AnF*, Anninghe Fault; *LxF*, Lijiang–Xiaojinhe Fault; *MlF*, Muli Fault; *JqF*, Jinhe–Qinghe Fault; *LzjF*, Lvzhijiang Fault; *YmF*, Yimen Fault; *PdF*, Pudu Fault; *XjF*, Xiaojiang Fault; *RrF*, Red River Fault; *AnR*, Anning River; *LcR*, Longchuan River; *PuR*, Pudu River; *LzR*, Lvzhi River; *NpR*, Nanpan River; *RrR*, Red River; *JsR*, Jinsha River; *LtR*, Litang River.

METHODS

The stream power incision model relates rock uplift and river incision over time along the longitudinal profile of the channel (Howard and Kerby, 1983; Howard et al., 1994), and it can be represented by **Eq. 1**:

$$\frac{\partial z}{\partial t} = U - KA^m\left(\frac{\partial z}{\partial x}\right)^n \tag{1}$$

where z represents the channel elevation, x represents the upstream distance, t represents time, U is the rock uplift rate, and K is the bedrock erodibility and is related to the channel width, the water discharge, the sediment load, and the lithologic resistance (Howard and Kerby, 1983; Howard et al., 1994). m and n are constant exponents, and A is the drainage area.

For a steady state, channel elevation at a particular point does not change, and then $\partial z/\partial t$ equals 0. From this, we can obtain **Eq. 2**.

$$\frac{dz}{dx} = k_s A^{-\theta} \tag{2}$$

$$K_s = \left(\frac{U}{K}\right)^{1/n} \tag{3}$$

$$\theta = \frac{m}{n} \tag{4}$$

where k_s and θ are the channel steepness and concavity indices, respectively. Generally, θ oscillated between 0.3 and 0.6 (Snyder et al., 2000; Snyder et al., 2006; Whipple, 2002; Kirby et al., 2003; Wobus et al., 2003). K_s is usually proportional to the rock uplift rates (**Eq. 3**). Although the longitudinal profile analysis was

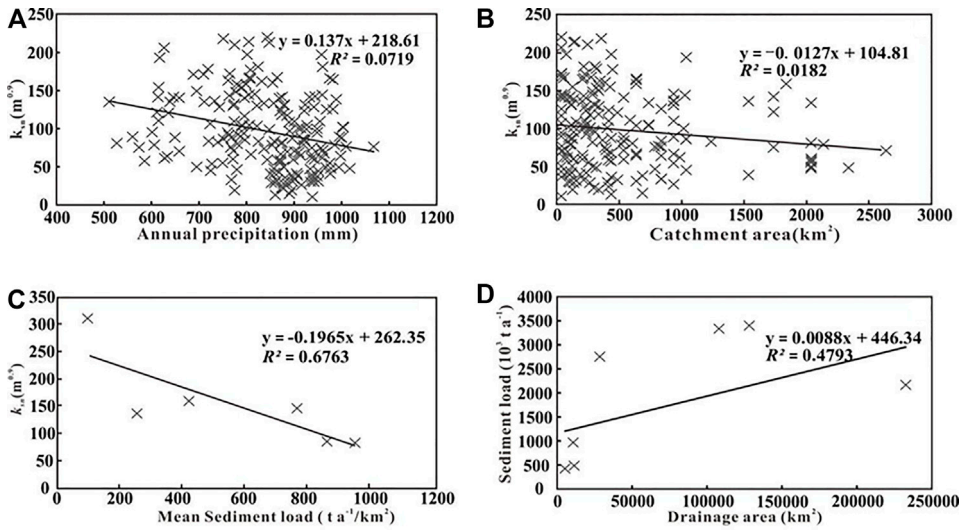

FIGURE 10 | Bi-variant linear regression of channel steepness (k_{sn})–annual precipitation **(A)**, channel steepness–catchment area **(B)**, mean sediment load–channel steepness **(C)**, and sediment load–drainage area **(D)**.

developed under steady-state assumptions, it has been extended to transient systems as well (e.g., Pan et al., 2015; Wang et al., 2017; Wang et al., 2019; Ma et al., 2020), and several studies (e.g., Snyder et al., 2000; Kirby et al., 2003; Wobus et al., 2003; Hu et al., 2010; Burbank and Anderson, 2011; Kirby and Whipple, 2012) showed that K_s is a useful index for denoting rock uplift rates at transient states.

θ can be gained by a log transformation to **Eq. 2** by Wobus et al. (2003).

$$\log\left(\frac{dz}{dx}\right) = -\theta \cdot \log(A) + \log(K_s) \tag{5}$$

The concavity and steepness indices are the slope and intercept of **Eq. 5**, respectively. K_s can be gained using **Eq. 6** (Perron and Royden, 2013).

$$z = z_b + \left(\frac{U}{KA_0^m}\right)^{\frac{1}{n}} \cdot \chi \tag{6}$$

$$\chi = \int_0^x \left(\frac{A_0}{A(x')}\right)^{\frac{m}{n}} dx' \tag{7}$$

where A_0 is the area factor and z_b is the channel elevation at river outlets ($x = 0$). $A_0/A_{(x)'}$ is dimensionless. Setting $A_0 = 1\ m^2$, the slope of **Eq. 6** is k_s.

We first used the ArcGIS 10.2 and MATLAB 2015b scripts (www.geomorphtools.org) to derive the concavity indices (**Figure 2**), steepness indices (**Figure 3**), and the longitudinal profiles (**Figures 4–6**). The steepness indices were determined using log*S*–log*A* plots according to the methods described by Wobus et al. (2003). Then, we interpolated the normalized channel steepness, k_{sn}, values of the river basins in the Central Yunnan subblock and created three swath profiles of the elevation and local steepness (**Figure 7**) (the profiles are E/W-directed, 220–350 km long and 20 km wide), finally presenting a distribution pattern over the Central Yunnan subblock. Due to the strong dependence of k_s on θ, a fixed reference concavity of 0.45 (a typical value used in many studies, e.g., Wobus et al., 2003; Hu et al., 2010; Perron and Royden, 2013) was used to generate *x*–*z* plots and to calculate the k_{sn} indices in order to compare the channels and channel segments of varying drainage areas (Whipple and Tucker, 1999). We resampled the elevation data at 20-m contour intervals with a 250-m smoothing window to decrease data noise (e.g., Wang et al., 2017).

RESULTS

In the Central Yunnan subblock, the 320 extracted river profiles had a mean concavity of 0.28 ± 0.063 (1σ), with a total range of 0.014–0.63 (**Figure 2**). In this section, however, we just described the most representative stream longitudinal profiles in the subblock (**Figures 3–7**). The detailed results are depicted in the **Supplementary Material** (**Supplementary Figure S1** and **Supplementary Table S1**). Furthermore, the k_{sn} and θ values are also listed in the **Supplementary Material** (**Supplementary Figure S1** and **Supplementary Table S1**).

In the northern areas controlled by a series of NE–SW thrust faults (such as the Jiulong and Muli thrust fault belts and the Jinhe–Qinghe thrust fault zone), these rivers had higher k_{sn} values (**Figure 3**), which can also be found from profile 1 (**Figure 7B**). The upper reaches of the Anning River also had high k_{sn} values, which may stem from their close proximity to areas of thrust faults (Muli Fault and Jinhe–Qinghe Fault) (**Figure 3**).

However, in the south areas controlled by the strike–slip faults and within the block, the rivers had lower k_{sn} values (**Figures 3**,

7). The lower reaches of the Anning River near the Xiaojiang strike–slip fault zone had low k_{sn} values. Similarly, the Pudu River and Lvzhi River and the Red River, which are close to the Pudu River Fault and Lvzhi River Fault, respectively, also had lower k_{sn} values in this area. From swath profiles 2 and 3, we can see that the k_{sn} values were low on both sides of the Xiaojiang fault zone, the Lvzhijiang Fault, and the Red River Fault and exhibited little change across the area (**Figures 7C, D**).

Based on the distribution pattern of the k_{sn} indices along the Central Yunnan subblock (**Figure 7A**), an approximate trend of change has been outlined, in which the average k_{sn} indices showed a general and gradual decrease from north to south.

DISCUSSION

The K_{sn} values were higher in the northern region controlled by the thrust faults and on both sides of the Jinsha River and were lower within the block and near strike–slip faults. The results suggest that the longitudinal river profiles correlated strongly with the underlying tectonic regime and may be used to make inferences regarding the tectonic setting or structure. However, if we want to attribute the variation of k_{sn} to the rock uplift rates, the influence of the lithology, precipitation, and sediment flux should be excluded.

Lithology

Channel bedrock erodibility is largely controlled by the lithologic resistance (Stock and Montgomery, 1999; Palumbo et al., 2010; Wang, 2014; Wang et al., 2018). As river incision through more resistant rocks (low K) requires greater stream power compared to less resistant rocks (high K), knickpoints are usually observed near the contact between rocks, with higher k_{sn} values in areas underlain by harder units (Duvall et al., 2004). Therefore, we analyzed the relationship between nine representative rivers with different lithologies (**Figures 5**, **6**) and their k_{sn} values to assess the influence of lithologic resistance.

Although the knickpoints observed along the Longchuan River (large-scale river, basin area $> 10^4$ km^2), C23 and Lz9 (middle-scale river, $10^3 <$ basin area $< 10^4$), are located near lithologic boundaries (**Figures 5**, **6**), the influences of variable lithologies on the channel profiles were weak. Along these rivers, the extracted k_{sn} values did not match the mapped lithologies (**Figure 8**). For example, in the lower reaches of the Anning River, although the lithology varied, we did not find an obvious knickpoint (**Figure 5**). But an obvious knickpoint was extracted from H20 (**Figure 6**), where the bedrock lithology of these channels is uniform.

Therefore, regional lithology does not appear to be a major influence on the channel profile of the subblock.

Precipitation

The effect of climate (mainly precipitation) on the channel profiles must be examined, as increased rates of rainfall often lead to increased river discharge and erosion of the bedrock beneath the channel. Ultimately, increased rainfall rates will decrease channel steepness, as channel steepness is often inversely proportional to the erodibility (**Eq. 3**). Here, the monthly precipitation data of 15 meteorological stations were collected from the China Meteorological Data Network (timescale: 1970–2019; downloaded from http://data.cma.cn) (**Figure 9**). These data were interpolated to derive the spatial distribution of average precipitation across the Central Yunnan subblock. The annual rainfall in the study area decreased from >1,200 mm (close to the Red River fault zone in the south) to <500 mm (close to the Lijiang–Xiaojinhe fault zone in the north) (**Figure 9**). This may be related to monsoons from the Indian Ocean being blocked by the Himalayas, promoting increased southeastern compared to northwestern rainfall. Increased runoff can be seen in the numerous river channels that have developed in Southwest China, such as the Yarlung Zangbo River Grand Canyon, the Lancang River Valley, the Jinsha River Valley, and other south-to-north valleys (Nie, 2018; Li, 1999).

From these data, there were two reasons to exclude precipitation as having a key role in controlling the k_{sn} values in the subblock. Firstly, by extracting the k_{sn} values from a small watershed in the study area, we found that the k_{sn} values in the northern part of the study area were higher than those in the southern part of the subblock (**Figure 7**). However, the rainfall in the southern part of the study area is higher than that in the northern part, which is inconsistent with our observation results of k_{sn} values (**Figure 9**). Secondly, we selected catchment basins with approximately 200 tributaries to quantify the relationship between rainfall and k_{sn} values. Rainfall in these basins ranges from 600 to 1,100 mm (**Figure 10A**), and the k_{sn} values had a wide range from 10.5 to 207 m$^{0.9}$. **Figure 10A** shows that the correlation between the k_{sn} values and precipitation was very weak ($R^2 = 0.0719$). As such, precipitation did not seem to control the distribution of k_{sn} values.

Sediment Flux

Abrupt changes in drainage area, water discharge, and sediment flux at tributary junctions might trigger knickpoint initiation. This behavior has been suggested in theoretical river incision models that included a dual sediment flux dependence (e.g., Gasparini and Brandon, 2011). In these models, the efficiency of bedrock incision increased with additional sediment flux up until the point when the increasing sediment no longer functioned as a tool to abrade the bed, but rather covered and armored the bed from further incision. The sediment flux in rivers mainly depends on the interplay between the actual total sediment flux (ATSF) and the river sediment capacity (RSC) (Willgoose, 1994; Tucker and Slingerland, 1996; Slingerland et al., 1997; Sklar and Dietrich, 2001; DiBiase et al., 2010). If ATSF < RSC, the materials carried by the river will erode the base of the river and increase the erosion rates (Wang et al., 2019). If ATSF > RSC, the material carried by the river will be deposited on the river bottom, thus protecting the riverbed from further erosion (Whipple, 2002) and lessening the rate at which the knickpoints move headwaters (Wang et al., 2019). As a result, the channel will become flatter and have a low concave.

Knickpoints along the Anning River (**Figure 8**) are located at the transition from the base of the channel, being characterized by

TABLE 1 | Locations of the hydrologic stations shown in **Figure 7**

Hydrologic station (hydropower station)	Drainage basin name	Sediment load (10^4 t annum^{-1})	Drainage area (km^2)	Record history	Channel steepness ($m^{0.9}$)
Tongzilin	Yalong	3,420	128,363	1954–1987	135
Xiaohuangguayuan	Longchuan	426	5,560	Multi-year average	146
Jiasa	Red River	2,772	28,816	Multi-year average	76.6
Wantan	Anning	973	11,037	1954–1987	81.3
Jiayan	Pudu	488.8	11,752	Multi-year average	160
Shigu	Jinsha	2,180	232,651	1954–1987	310

sediment characterized by bedrock. However, the k_{sn} values across the Central Yunnan subblock are not controlled by sediment flux.

We compared the k_{sn} and concavity values extracted for each class of lithology through a statistical analysis derived from **Figure 2**. Comparison of the concavity and k_{sn} values showed no linear relationship. In a normalized height–distance coordinate system, the concavity indices are close to a constant and represent similar channel shapes (Whipple and Tucker, 1999; Duvall et al., 2004; Kirby and Whipple, 2012).

The records of sediment load and drainage area were from Qin et al. (2019) and Pan (1997). Channel steepness values are shown in **Figure 6**.

We also found no systematic change of the k_{sn} values with varying sediment concentrations and the basin area. We obtained the sediment load data (including bed load, suspended load, and solute) from hydrological stations and hydroelectric stations of the Central Yunnan subblock and calculated the k_{sn} values of the channel portions downstream of the knickpoints (**Table 1**) (Pan, 1997; Qin et al., 2019). The soil erosion modulus of the Jinsha River basin in Yunnan is 1,530 t/km^2 (Huang et al., 2006), and the calculated sediment transport capacity is far greater than the actual sediment transport capacity. We found no obvious relevance between the watershed area and the k_{sn} values in the tributary catchments ($R^2 = 0.0182$) (**Figure 10B**). The calculated sediment transport capacity is far greater than the actual sediment transport. Therefore, k_{sn} should increase with the increase of the mean sediment load, but the trend cannot be seen from **Figure 10C**. Despite limited data, the sediment loads increased with the watershed area ($R^2 = 0.4793$) (**Figure 10D**).

Therefore, sediment flux did not appear to have dominant control on the k_{sn} value in the channel profile.

Patterns of Rock Uplift

Non-tectonic factors (e.g., lithologic resistance, precipitation, and sediment flux) could not fully explain the k_{sn} distribution. The most active areas of the interpreted uplift are scattered in the region controlled by the NE/SW-trending thrust faults in the north of the Central Yunnan subblock. Therefore, the distribution of the k_{sn} values is likely tectonically controlled.

The Xianshuihe–Xiaojiang Fault accommodates the shortage from the India–Eurasia collision by the left lateral strike–slip motion (e.g., Molnar and Tapponnier, 1975; Molnar et al., 1987; Deng et al., 2002; Xu et al., 2003; Wen et al., 2003). Since 13 Ma, the maximum slip rate of the north part of the Xiaojiang fault system has reached up to 10 mm/annum (Xu et al., 2003), and this rate has decreased progressively southward. At the south end of the Xiaojiang Fault, no obvious slip can be found (Wang et al., 1998). In the growth model for the Tibetan Plateau of Tapponnier et al. (1982) and Tapponnier (2001), the strain was mainly localized along the boundary faults of large blocks (Tapponnier, 2001). Fast erosion rates in the adjacent zone of the strike–slip fault belt can be found (Wang et al., 2017; 2021); however, the k_{sn} values were low on both sides of the strike–slip faults and exhibited little change across the area (**Figure 7A**). This may be due to the limited vertical slip and fast strike–slip rate (Molnar and Tapponnier, 1975; Molnar et al., 1987; Deng et al., 2002; Xu et al., 2003) in the strike–slip fault zone (Zhang, 2008; Wu et al., 2014).

Along the transition between the Xianshuihe Fault and Xiaojiang Fault, some active thrust faults with a NE trend were cut by this Xianshuihe–Xiaojiang Fault and propagated southwestward (**Figure 1**). Slip vector analyses argued that the sinistral slip rates from west to east across these thrust faults have decreased (Xu et al., 2003). Their loss has been considered to be transformed into local crustal shortening perpendicular to the active thrust faults. As a result, the distribution pattern of k_{sn} along the Xiaojiang Fault, obtained in this study, is in good agreement with the thrusting transformation-limited extrusion model of the Tibetan Plateau.

The slope–area regression of the longitudinal profiles revealed that the rock uplift in the interior of the block is lower compared to the north part controlled by a series of NE–NW thrust faults (such as the Jiulong, Muli, and Jinhe–Qinghe thrust faults) where rivers have high k_{sn} values and contain several knickpoints along their profiles, suggesting that the tectonic signals have propagated upstream in the landscape by knickpoint recession. This process resulted in higher indices in the downstream, along trunk and tributary channels (Wang et al., 2017; Zhang et al., 2020). The lower part of the Jinsha River trunk also showed high channel steepness, and the region east of the Xianshuihe Fault also had high channel steepness, although distant from the thrust faults, which appears to be the products of the knickpoint recession (Zhang et al., 2022).

We postulated that, in the interior of the block, the rivers experienced successive base-level uplifts that have migrated upslope, reaching the headwater (e.g., Clark et al., 2005; Schoenbohm et al., 2006; Royden et al., 2008; Wang et al., 2017). The distribution of lower k_{sn} values at the headwaters, the unperturbed reaches with a tight slope–area regression with low k_{sn} values, suggest that, in the growth model for the Tibetan Plateau of Tapponnier et al. (1982) and Tapponnier (2001), the

great crustal shortening between the Indian and Eurasian plates was mainly absorbed by a series of strike–slip fault systems and the related thrust faults.

CONCLUSION

In this study, we calculated the distribution pattern of normalized channel steepness by the stream power incision model of 300 rivers in the Central Yunnan subblock. The distribution pattern has been clearly observed to represent a general increase in value from north to south in this subblock. Higher k_{sn} values were associated with the NE/SW-trending Cenozoic thrust faults (including the Muli Fault, Lijiang–Xiaojinhe Fault, and Jinhe–Qihe Fault). Lower k_{sn} values were found on both sides of the Xiaojiang fault zone and the Red River fault zone. The influences of non-tectonic factors were discussed and excluded. We suggested that very weak correlations were found between the steepness indices and the lithology, precipitation, sediment flux, or channel concavity indices. Along the Xiaojiang strike–slip fault and the interior subblock, the uplift rate was slower, while the northern part had uplifted faster and was controlled by thrust fault systems. The channel steepness increased gradually from south to north. Thus, the distribution pattern of the K_{sn} index within the Central Yunnan subblock provides notable support for the argument for the thrusting transformation-limited extrusion model of the Tibetan Plateau.

DATA AVAILABILITY STATEMENT

The original contributions presented in the study are included in the article/**Supplementary Material**, further inquiries can be directed to the corresponding authors.

AUTHOR CONTRIBUTIONS

LY and YD conceived of the presented idea. YD and WZ developed the theoretical framework. LY, DZ, and DW developed the theory, analyzed the data, and performed the computations. HY, YR, and JL verified the analytical methods. All authors discussed the results and contributed to the final manuscript.

FUNDING

This study is supported by the National Natural Science Foundation of China (nos. 41802215 and 41762017).

SUPPLEMENTARY MATERIAL

The Supplementary Material for this article can be found online at: https://www.frontiersin.org/articles/10.3389/feart.2022.821367/full#supplementary-material

REFERENCES

Allen, G. H., Barnes, J. B., Pavelsky, T. M., and Kirby, E. (2013). Lithologic and Tectonic Controls on Bedrock Channel Form at the Northwest Himalayan Front. *J. Geophys. Res. Earth Surf.* 118 (3), 1806–1825. doi:10.1002/jgrf.20113

Burbank, D. W., and Anderson, R. S. (2011). *Tectonic Geomorphology*. Massachusetts: Blackwell Science, 247–251.

Burchfiel, B. C., Zhiliang, C., Yupinc, L., and Royden, L. H. (1995). Tectonics of the Longmen Shan and Adjacent Regions, Central China. *Int. Geology. Rev.* 37, 661–735. doi:10.1080/00206819509465424

Chen, W., Zhan, Y., Zhang, Y. Q., Jin, G. S., and Wang, Q. L. (2006). Late Cenozoic Episodic Uplifting in southeastern Part of the Tibetan Plateau - Evidence from Ar-Ar Thermochronology. *Acta Petrologica Sinica.* 73 (4), A1512. doi:10.1016/j.sedgeo.2005.11.021

Clark, M. K., Schoenbohm, L. M., Royden, L. H., Whipple, K. X., Burchfiel, B. C., Zhang, X., et al. (2004). Surface Uplift, Tectonics, and Erosion of Eastern Tibet from Large-Scale Drainage Patterns. *Tectonics.* 23 (1), 6. doi:10.1029/2002tc001402

Clark, M. K. (2012). Continental Collision Slowing Due to Viscous Mantle Lithosphere rather Than Topography. *Nature.* 483 (7387), 74–77. doi:10.1038/nature10848

Clark, M. K., House, M. A., Royden, L. H., Whipple, K. X., Burchfiel, B. C., Zhang, X., et al. (2005). Late Cenozoic Uplift of Southeastern Tibet. *Geol.* 33 (6), 525–528. doi:10.1130/g21265.1

Deng, Q., Zhang, P., Ran, Y., Yang, X., Min, W., and Chu, Q. (2002). Basic Characteristics of Active Tectonics of China. *Sci. China Ser. D Earth Sci.* 32 (12), 1020–1030. doi:10.3969/j.issn.1674-7313.2003.04.005

Dibiase, R. A. (2014). River Incision Revisited. *Nature.* 505 (7483), 294–295. doi:10.1038/505294a

DiBiase, R. A., Whipple, K. X., Heimsath, A. M., and Ouimet, W. B. (2010). Landscape Form and Millennial Erosion Rates in the San Gabriel Mountains, CA. *Earth Planet. Sci. Lett.* 289 (1-2), 134–144. doi:10.1016/j.epsl.2009.10.036

Dibiase, R. A., and Whipple, K. X. (2011). The Influence of Erosion Thresholds and Runoff Variability on the Relationships Among Topography, Climate, and Erosion Rate. *J. Geophys. Res. Earth Surf.* 116 (F4), F04036. doi:10.1029/2011jf002095

Duvall, A., Kirby, E., and Burbank, D. (2004). Tectonic and Lithologic Controls on Bedrock Channel Profiles and Processes in Coastal California. *J. Geophys. Res. Earth Surf.* 109 (F3), F03002. doi:10.1029/2003jf000086

Ferrier, K. L., Huppert, K. L., and Perron, J. T. (2013). Climatic Control of Bedrock River Incision. *Nature.* 496 (7444), 206–209. doi:10.1038/nature11982

Finnegan, N., Schumer, R., and Finnegan, S. (2014). A Signature of Transience in Bedrock River Incision Rates over Timescales of 10^4–10^7 Years. *Nature* 505 (7483), 391. doi:10.1038/nature12913

Gasparini, N. M., and Brandon, M. T. (2011). A Generalized Power Law Approximation for Fluvial Incision of Bedrock Channels. *J. Geophys. Res.* 116, F02020. doi:10.1029/2009jf001655

Hartshorn, K., Hovius, N., Dade, W. B., and Slingerland, R. L. (2002). Climate-Driven Bedrock Incision in an Active Mountain Belt. *Science.* 297 (5589), 2036–2038. doi:10.1126/science.1075078

He, J., Lu, S., and Wang, X. (2009). Mechanical Relation between Crustal Rheology, Effective Fault Friction, and Strike-Slip Partitioning Among the Xiaojiang Fault System, southeastern Tibet. *J. Asian Earth Sci.* 34 (3), 363–375. doi:10.1016/j.jseaes.2008.06.003

Hoke, G. D. (2018). Geochronology Transforms Our View of How Tibet's Southeast Margin Evolved. *Geology (Boulder).* 46 (1), 95–96. doi:10.1130/focus012018.1

Houseman, G., and England, P. (1993). Crustal Thickening versus Lateral Expulsion in the Indian-Asian continental Collision. *J. Geophys. Res.* 98 (B7), 12233–12249. doi:10.1029/93jb00443

Howard, A. D., Dietrich, W. E., and Seidl, M. A. (1994). Modeling Fluvial Erosion on Regional to continental Scales. *J. Geophys. Res.* 99 (B7), 13971–13986. doi:10.1029/94jb00744

Howard, A. D., and Kerby, G. (1983). Channel Changes in Badlands. *Geol. Soc. America Bull.* 94 (6), 739–752. doi:10.1130/0016-7606(1983)94<739:ccib>2.0.co;2

Hu, X., Pan, B., Kirby, E., Li, Q., and GengChen, H. J. (2010). Spatial Differences in Rock Uplift Rates Inferred from Channel Steepness Indices along the Northern Flank of the Qilian Mountain, Northeast Tibetan Plateau. *Chin. Sci. Bull.* 55 (27–28), 3205–3214. doi:10.1007/s11434-010-4024-4

Huang, Y., Guo, Y., and Fang, S. (2006). "Analysis on the Variation Characteristics of Water and Sediment in Jinsha River Basin in Yunnan Province, Chinese Hydraulic Society 2006 Annual Conference and 2006 Hydrology Symposium," in Proceedings of 2006 Annual Conference of Chinese Hydraulic Society and 2006 Hydrology Symposium (Application of New Technologies in Hydrology and Water Resources) (Anhui Province, China: Hefei), 6.

Huangfu, G., and Qin, J. (2006). Study of the Seismicity of Strong Earthquakes in the Yunnan Area. *Earthq. res. China* 28 (1), 37–47.

Kirby, E., Johnson, C., and Heimsath, A. (2007). Transient Channel Incision along Bolinas Ridge, California: Evidence for Differential Rock Uplift Adjacent to the San Andreas Fault. *J. Geophys. Res. Earth Surf.* 112, F03S07. doi:10.1029/2006jf000559

Kirby, E., and Ouimet, W. (2011). Tectonic Geomorphology along the Eastern Margin of Tibet: Insights into the Pattern and Processes of Active Deformation Adjacent to the Sichuan Basin. *Geol. Soc. Lond. Spec. Publications.* 353 (1), 358–361. doi:10.1144/sp353.9

Kirby, E., and Whipple, K. (2001). Quantifying Differential Rock-Uplift Rates via Stream Profile Analysis. *Geol.* 29 (5), 415–418. doi:10.1130/0091-7613(2001)029<0415:qdrurv>2.0.co;2

Kirby, E., and Whipple, K. X. (2012). Expression of Active Tectonics in Erosional Landscapes. *J. Struct. Geology.* 44, 54–75. doi:10.1016/j.jsg.2012.07.009

Kirby, E., Whipple, K. X., Tang, W. Q., and Chen, Z. L. (2003). Distribution of Active Rock Uplift along the Eastern Margin of the Tibetan Plateau: Inferences from Bedrock Channel Longitudinal Profiles. *J. Geophys. Res. Solid Earth.* 108 (B4), 2217. doi:10.1029/2001jb000861

Lavé, J., and Avouac, J. P. (2001). Fluvial Incision and Tectonic Uplift Across the Himalayas of central Nepal. *J. Geophys. Res.* 106 (B11), 26561–26591. doi:10.1029/2001jb000359

Li, H., and Zhang, Y. (2013). Zircon U-Pb Geochronology of the Konggar Granitoid and Migmatite: Constraints on the Oligo-Miocene Tectono-Thermal Evolution of the Xianshuihe Fault Zone, East Tibet. *Tectonophysics.* 606, 127–139. doi:10.1016/j.tecto.2013.07.007

Li, S., Currie, B., Rowley, D., and Ingalls, M. (2015). Cenozoic Paleoaltimetry of the SE Margin of the Tibetan Plateau: Constraints on the Tectonic Evolution of the Region. *Earth Planet. Sci.* 432, 415–424. doi:10.1016/j.epsl.2015.09.044

Li, J. (1999). Studies of the Geomorphological Evolution of the Qinghai-Xizang (Tibetan) Plateau and Asian Monsoon. *Mar. Geol. Quater. Geol.* 19 (2), 1–12.

Liu, J., Zeng, L., Ding, L., Tapponnier, P., Gaudemer, Y., Wen, L., et al. (2009). Tectonic geomorphology, active tectonics and lower crustal channel flow hypothesis of the southeastern Tibetan Plateau. *Journal of Geology (Scientia Geologica Sinica)* 44 (4), 1227–1255. doi:10.3321/j.issn:0563-5020.2009.04.014

Liu, Z. J., Tapponnier, P., Gaudemer, Y., and Ding, L. (2008). Quantifying Landscape Differences across the Tibetan Plateau: Implications for Topographic Relief Evolution. *J. Geophys. Res. Earth Surf.* 113 (F4), F04018. doi:10.1029/2007jf000897

Liu-Zeng, J., Zhang, J., McPhillips, D., Reiners, P., Wang, W., Pik, R., et al. (2018). Multiple Episodes of Fast Exhumation since Cretaceous in Southeast Tibet, Revealed by Low-Temperature Thermochronology. *Earth Planet. Sci. Lett.* 490 (15), 62–76. doi:10.1016/j.epsl.2018.03.011

Ma, Z., Zhang, H., Wang, Y., Tao, Y., and Li, X. (2020). Inversion of Dadu River Bedrock Channels for the Late Cenozoic Uplift History of the Eastern Tibetan Plateau. *Geophys. Res. Lett.* 47, e2019GL086882. doi:10.1029/2019gl086882

Molnar, P., Burchfiel, B. C., K'uangyi, L., and Ziyun, Z. (1987). Geomorphic Evidence for Active Faulting in the Altyn Tagh and Northern Tibet and Qualitative Estimates of its Contribution to the Convergence of India and Eurasia. *Geol.* 15 (3), 249–253. doi:10.1130/0091-7613(1987)15<249:gefafi>2.0.co;2

Molnar, P., and England, P. (1990). Late Cenozoic Uplift of Mountain Ranges and Global Climate Change: Chicken or Egg? *Nature.* 346 (6279), 29–34. doi:10.1038/346029a0

Molnar, P., and Tapponnier, P. (1975). Cenozoic Tectonics of Asia: Effects of a Continental Collision: Features of Recent continental Tectonics in Asia Can Be Interpreted as Results of the India-Eurasia Collision. *Science.* 189, 419–426. doi:10.1126/science.189.4201.419

Nie, J. (2018). Rapid Incision of the Mekong River in the Middle Miocene Linked to Monsoonal Precipitation. *Nat. Geoence.* 11, 944. doi:10.1038/s41561-018-0244-z

Oskin, M. E., Burbank, D. W., Phillips, F. M., Marrero, S. M., Bookhagen, B., and Selander, J. A. (2014). Relationship of Channel Steepness to Channel Incision Rate from a Tilted and Progressively Exposed Unconformity Surface. *J. Geophys. Res. Earth Surf.* 119 (2), 366–384. doi:10.1002/2013jf002826

Palumbo, L., Hetzel, R., Tao, M., and Li, X. (2010). Topographic and Lithologic Control on Catchment-Wide Denudation Rates Derived from Cosmogenic 10Be in Two Mountain Ranges at the Margin of NE Tibet. *Geomorphology.* 117 (1-2), 130–142. doi:10.1016/j.geomorph.2009.11.019

Pan, B., Li, Q., Hu, X., Geng, H., and Gao, H. (2015). Bedrock Channels Response to Differential Rock Uplift in Eastern Qilian Mountain along the Northeastern Margin of the Tibetan Plateau. *J. Asian Earth Sci.* 100, 1–19. doi:10.1016/j.jseaes.2014.12.009

Pan, J. (1997). Study on Sediment Transport Characteristics in Jinsha River Basin. *Bull. soll Water conservation.* 17 (5), 35–39. doi:10.13961/j.cnki.stbctb.1997.05.008

Perron, J. T., and Royden, L. (2013). An Integral Approach to Bedrock River Profile Analysis. *Earth Surf. Process. Landforms.* 38 (6), 570–576. doi:10.1002/esp.3302

Pritchard, D., Roberts, G. G., White, N. J., and Richardson, C. N. (2009). Uplift Histories from River Profiles. *Geophys. Res. Lett.* 36 (24), L24301. doi:10.1029/2009gl040928

Qin, L., Dong, X., Du, Z., and Chen, X. (2019). Processes of Water-Sediment and Deposition in cascade Reservoirs in the Lower Reach of Jinsha River. *J. Sediment Res.* 44 (03), 24–30. doi:10.16239/j.cnki.0468-155x.2019.03.005

Raymo, M. E., and Ruddiman, W. F. (1992). Tectonic Forcing of Late Cenozoic Climate. *Nature.* 359 (6391), 117–122. doi:10.1038/359117a0

Royden, L., Burchfiel, B., and Hilst, R. (2008). The Geological Evolution of the Tibetan Plateau. *Science* 321 (5892), 1054–8. doi:10.1126/science.1155371

Royden, L. H., Burchfiel, B. C., King, R. W., Wang, E., Chen, Z., Shen, F., et al. (1997). Surface Deformation and Lower Crustal Flow in Eastern Tibet. *Science.* 276 (5313), 788–790. doi:10.1126/science.276.5313.788

Schoenbohm, L., Burchfiel, B. C., and Chen, L. (2006). Propagation of Surface Uplift, Lower Crustal Flow, and Cenozoic Tectonics of the Southeast Margin of the Tibetan Plateau. *Geology* 34, 813–816. doi:10.1130/G22679.1

Schwanghart, W., and Scherler, D. (2020). Divide Mobility Controls Knickpoint Migration on the Roan Plateau (Colorado, USA). *Geology.* 48 (7), 698. doi:10.1130/g47054.1

Shen, X., Tian, Y., Li, D., Qin, S., Vermeesch, P., and Schwanethal, J. (2016). Oligocene-Early Miocene River Incision Near the First bend of the Yangze River: Insights from Apatite (U-Th-Sm)/He Thermochronology. *Tectonophysics.* 687, 223–231. doi:10.1016/j.tecto.2016.08.006

Sklar, L. S., and Dietrich, W. E. (2001). Sediment and Rock Strength Controls on River Incision into Bedrock. *Geol.* 29 (12), 1087–1090. doi:10.1130/0091-7613(2001)029<1087:sarsco>2.0.co;2

Slingerland, R., Willett, S. D., and Hennessey, L. H. (1997). A New Fluvial Bedrock Erosion Model Based on the Work-Energy Principle. *Eos Trans. AGU* 78 (46), Suppl., F299.

Snyder, E., Johnson, N., Spyropolou, J., Crosby, K., and Sheehan, D. (2006). Tectonics from Topography: Procedure, Promise, and Pitfalls. *Geol. Soc. Am. Spec.* 398 (12), 55–74. doi:10.1130/2006.2398(04)

Snyder, N. P., Whipple, K. X., Tucker, G. E., and Merritts, D. J. (2000). Landscape Response to Tectonic Forcing: Digital Elevation Model Analysis of Stream Profiles in the Mendocino Triple junction Region, Northern California. *Geol. Soc. America Bull.* 112 (8), 1250–1263. doi:10.1130/0016-7606(2000)112<1250:lrttfd>2.0.co;2

Stock, J. D., and Montgomery, D. R. (1999). Geologic Constraints on Bedrock River Incision Using the Stream Power Law. *J. Geophys. Res. Solid Earth.* 104 (B3), 4983. doi:10.1029/98jb02139

Su, Q., Yuan, D., and Xie, H. (2016). Geomorphic Features of the Heihe River Drainage basin in Western Qilian Shan-Hexi Corridor and its Tectonicimplications. *Seismology Geology* 38 (3), 560–581. doi:10.3969/j.issn.0253-4967.2016.03.005

Tang, M., Liu-Zeng, J., Hoke, G. D., Xu, Q., Wang, W., Li, Z., et al. (2017). Paleoelevation Reconstruction of the Paleocene-Eocene Gonjo basin, SE-central Tibet. *Tectonophysics.* 712-713, 170–181. doi:10.1016/j.tecto.2017.05.018

Tapponnier, P., Peltzer, G., and Le Dain, A. Y. (1982). Propagating Extrusion Tectonics in Asia, New Insights from Simple Experiments with Plasticine. *Geology* 10 (12), 611–617. doi:10.1130/0091-7613(1982)10<611:PETIAN>2.0.CO;2

Tapponnier, P., Zhiqin, X., Roger, F., Meyer, B., Arnaud, N., Wittlinger, G., et al. (2001). Oblique Stepwise Rise and Growth of the Tibet Plateau. *Science.* 294 (5547), 1671–1677. doi:10.1126/science.105978

Tian, Y., Kohn, B. P., Gleadow, A. J. W., and Hu, S. (2014). A Thermochronological Perspective on the Morphotectonic Evolution of the southeastern Tibetan Plateau. *J. Geophys. Res. Solid Earth.* 119 (1), 676–698. doi:10.1002/2013jb010429

Tian, Y., Kohn, B. P., Hu, S., and Gleadow, A. J. W. (2015). Synchronous Fluvial Response to Surface Uplift in the Eastern Tibetan Plateau: Implications for Crustal Dynamics. *Geophys. Res. Lett.* 42, 29. doi:10.1002/2014gl062383

Tian, Y. T., Kohn, B. P., and Gleadow, A. J. W. (2013). Constructing the Longmenshan Eastern Tibetan Plateau Margin: Insights from Low-Temperature Thermochronology. *Tectonics.* 32, 572–596. doi:10.1002/tect.20043

Tucker, G. E., and Slingerland, R. (1996). Predicting Sediment Flux from Fold and Thrust Belts. *Basin Res.* 8 (3), 329–349. doi:10.1046/j.1365-2117.1996.00238.x

Wang, E., Burchfiel, B. C., Royden, L. H., Chen, L., Chen, J., Li, W., et al. (1998). *The Cenozoic Xianshuihe–Xiaojiang,Red River, and Dali Faultsystems of Southwestern Sichuan and central Yunnan*, 327. China: Geological Society of America Special Paper, 108.

Wang, F., Wang, M., Wang, Y., and Shen, Z.-K. (2015). Earthquake Potential of the Sichuan-Yunnan Region, Western China. *J. Asian Earth Sci.* 107, 232–243. doi:10.1016/j.jseaes.2015.04.041

Wang, S., Jiang, G., Xu, T., Tian, Y., Zheng, D., and Fang, X. (2012). The Jinhe–Qinghe Fault-An Inactive branch of the Xianshuihe–Xiaojiang Fault Zone, Eastern Tibet. *Tectonophysics* 544545, 93–102.

Wang, Y., Liu, C., Zheng, D., Zhang, H., Yu, J., Pang, J., et al. (2021). Multistage Exhumation in the Catchment of the Anninghe River in the SE Tibetan Plateau: Insights from Both Detrital Thermochronology and Topographic Analysis. *Geophys. Res. Lett.*, 48. doi:10.1029/2021GL092587

Wang, Y., Schoenbohm, L. M., Zhang, B., Granger, D. E., Zhou, R., Zhang, J., et al. (2017). Late Cenozoic Landscape Evolution along the Ailao Shan Shear Zone, SE Tibetan Plateau: Evidence from Fluvial Longitudinal Profiles and Cosmogenic Erosion Rates. *Earth Planet. Sci. Lett.* 472 (1), 323–333. doi:10.1016/j.epsl.2017.05.030

Wang, Y. Z. (2014). Controls on Decadal Erosion Rates in Qilian Shan: Re-evaluation and New Insights into Landscape Evolution in north-east Tibet. *Geomorphology.* 223 (October15), 117–128. doi:10.1016/j.geomorph.2014.07.002

Wang, Y., Zheng, D., Pang, J., Zhang, H., Wang, W., Yu, J., et al. (2018). Using Slope-Area and Apatite Fission Track Analysis to Decipher the Rock Uplift Pattern of the Yumu Shan: New Insights into the Growth of the NE Tibetan Plateau. *Geomorphology.* 308 (MAY1), 118–128. doi:10.1016/j.geomorph.2018.02.006

Wang, Y., Zheng, D., Zhang, H., Li, C., Xiao, L., Li, Y., et al. (2019). The Distribution of Active Rock Uplift in the interior of the Western Qilian Shan, NE Tibetan Plateau: Inference from Bedrock Channel Profiles. *Tectonophysics.* 759, 15–29. doi:10.1016/j.tecto.2019.04.001

Wen, X., Xu, X., and Zheng, R. (2003). Average Slip-Rate and Recent Large Earthquake Ruptures along the Garzê-Yushu Fault. *Sci. China Earth Sci.* 46 (0z2), 276–288. doi:10.1360/03dz0022

Whipple, K. X. (2004). Bedrock Rivers and the Geomorphology of Active Orogens. *Annu. Rev. Earth Planet. Sci.* 32, 151–185. doi:10.1146/annurev.earth.32.101802.120356

Whipple, K. X. (2002). Implications of Sediment-flux-dependent River Incision Models for Landscape Evolution. *J. Geophys. Res.* 107 (B2), 2039. doi:10.1029/2000jb000044

Whipple, K. X., and Tucker, G. E. (1999). Dynamics of the Stream-Power River Incision Model: Implications for Height Limits of Mountain Ranges, Landscape Response Timescales, and Research Needs. *J. Geophys. Res.* 104 (B8), 17661–17674. doi:10.1029/1999jb900120

Willgoose, G. (1994). A Physical Explanation for an Observed Area-slope-elevation Relationship for Catchments with Declining Relief. *Water Resour. Res.* 30, 151. doi:10.1029/93wr01810

Wilson, C., and Fowler, A. P. (2011). Denudational Response to Surface Uplift in East Tibet: Evidence from Apatite Fission-Track Thermochronology. *Geol. Soc. America Bull.* 123 (9-10), 1966–1987. doi:10.1130/b30331.1

Wobus, C., Whipple, K., Kirby, E., Snyder, N., Jhonson, J., Spyropolou, K., et al. (2006). Tectonics From Topography: Procedures, Promise, and Pitfalls. *Geol. Soc. Am. Spec. Pap.* 398, 55–74. doi:10.1130/2006.2398(04)

Wobus, C. W., Hodges, K. V., and Whipple, K. X. (2003). Has Focused Denudation Sustained Active Thrusting at the Himalayan Topographic Front? *Geol.* 31 (10), 861–864. doi:10.1130/g19730.1

Wu, Z., Zhou, C., Feng, H., Zhang, K., Li, J., Ye, P., et al. (2014). Active Faults and Earthquake Around Yushu in Eastern Tibetan Plateau. *Geological Bulletin of China* 33 (4), 419–469.

Wu, K., Dong, Y., Duan, J., Ru, X., Zhang, D., and Wang, D. (2020). Cenozoic Uplift of the Central Yunnan Fragment, Southwestern China, Revealed by Apatite. *J. Earth Sci.* 31 (04), 735–742. doi:10.1007/s12583-020-1328-4

Xiang, H., Xu, X., Guo, S., Zhang, W., Li, H., and Yu, G. (2002). Sinistaral Thrusting along the Lijiang-Xiaojinhe Fault since Quaternary and its Geologic-Tectonic Significance-Shielding Effect of Transverse Structure of Intracontinental Active Block. *Seismoseismology Geology.* 24 (2), 188–198. doi:10.1080/12265080208422884

Xu, G., and Kamp, P. J. J. (2000). Tectonics and Denudation Adjacent to the Xianshuihe Fault, Eastern Tibetan Plateau: Constraints from Fission Track Thermochronology. *J. Geophys. Res.* 105, 19231–19251. doi:10.1029/2000jb900159

Xu, X., Cheng, G., Yu, G., Song, F. M., and Wen, X. Z. (2003). Tectonic and Paleomagnetic Evidence for the Clockwise Rotation of the Sichuan-Yunnan Rhombic Block. *Seismology Geology.* 25 (1), 61–70. doi:10.1016/S0955-2219(02)00073-0

Xu, Z., Yang, J., Li, H., Zhang, J., and Wu, C. (2007). *Orogenic Plateaux-Terrane Amalgamation, Collision and Uplift in the Qinghai-Tibet Plateau*. Beijing, China: Geological Publishing House, 1–458. doi:10.1130/2006.2398(04)

Yan, B., and Lin, A. (2015). Systematic Deflection and Offset of the Yangtze River Drainage System along the Strike-Slip Ganzi-Yushu-Xianshuihe Fault Zone, Tibetan Plateau. *J. Geodynamics.* 87, 13–25. doi:10.1016/j.jog.2015.03.002

Yin, Q., Li, H., and Wang, Q. (2020). The Study of the Dextral Oblique-Slip Deformation of the Jinhe-Qinghe Fault, Southeast Tibet, and its Tectonic Significance. *Acta Geoscientica Sinica.* 41 (3), 371–383. doi:10.3975/cagsb.2020.012201

Zhang, L., Li, T., Wang, G., Kwang, J., Parker, G., et al. (2020). How Canyons Evolve by Incision into Bedrock: Rainbow Canyon, Death Valley National Park, United States. *Proc. Natl. Acad. Sci.* 117 (26), 201911040. doi:10.1073/pnas.1911040117

Zhang, D., Dong, Y., Jiao, Q., Duan, J., Wang, D., Yu, L., et al. (2022). Three Periods of Cenozoic Tectonic Uplift in the Southeastern Margin of the Tibetan Plateau-Evidence from Fluvial Longitudinal Profile Analysis. *Geotectonic Et Metallogenia.* In press.

Zhang, P. (2008). The Current Tectonic Deformation, Strain Distribution and Deep Dynamic Process in Western Sichuan Province in the East of Qinghai-Tibet Plateau. *Science in China Series D-Earth Sciences (in Chinese)* 38 (9), 1041–1056.

Zhang, H., Oskin, M., Oskin, M. E., Liu-Zeng, J., Zhang, P., Reiners, P. W., et al. (2016). Pulsed Exhumation of interior Eastern Tibet: Implications for Relief Generation Mechanisms and the Origin of High-Elevation Planation Surfaces.

Earth Planet. Sci. Lett. 449 (September1), 176–185. doi:10.1016/j.epsl.2016.05.048

Zhang, Y.-Z., Replumaz, A., Replumaz, A., Leloup, P. H., Wang, G.-C., Bernet, M., et al. (2017). Cooling History of the Gongga Batholith: Implications for the Xianshuihe Fault and Miocene Kinematics of SE Tibet. *Earth Planet. Sci. Lett.* 465, 1–15. doi:10.1016/j.epsl.2017.02.025

Zheng, H., Clift, P. D., Wang, P., Tada, R., Jia, J., He, M., et al. (2013). Pre-Miocene Birth of the Yangtze River. *Proc. Natl. Acad. Sci. U S A.* 110 (19), 7556–7561. doi:10.1073/pnas.1216241110

Conflict of Interest: The authors declare that the research was conducted in the absence of any commercial or financial relationships that could be construed as a potential conflict of interest.

Publisher's Note: All claims expressed in this article are solely those of the authors and do not necessarily represent those of their affiliated organizations, or those of the publisher, the editors and the reviewers. Any product that may be evaluated in this article, or claim that may be made by its manufacturer, is not guaranteed or endorsed by the publisher.